# Chemomechanical properties and microstructural stability of nanocrystalline Pr-doped ceria: An *in situ* X-ray diffraction investigation

Y. Kuru [a,b,*], S.R. Bishop [a], J.J. Kim [a], B. Yildiz [b], H.L. Tuller [a]

[a] *Department of Materials Science & Engineering, Massachusetts Institute of Technology, 77 Massachusetts Avenue, Cambridge, MA 02139, USA*
[b] *Department of Nuclear Science & Engineering, Massachusetts Institute of Technology, 77 Massachusetts Avenue, Cambridge, MA 02139, USA*

## ARTICLE INFO

## ABSTRACT

The chemomechanical properties and microstructural stability of nanocrystalline $Pr_xCe_{1-x}O_{2-\delta}$ solid solutions are studied as a function of temperature by *in situ* X-ray diffraction measurements under oxidizing conditions at $P(O_2) \sim 200$ mbar. The chemical expansion coefficient of nanocrystalline powder specimens, operative at intermediate temperatures during which $Pr^{4+}$ is reduced to $Pr^{3+}$, is found to be similar to that obtained for coarse-grained $Pr_xCe_{1-x}O_{2-\delta}$. This is contrary to reports regarding variation of physical and chemical properties with crystallite size. The thermal expansion coefficient, measured under conditions for which $Pr_xCe_{1-x}O_{2-\delta}$ is highly oxygen deficient, was found to be greater than that measured for fully oxidized $Pr_xCe_{1-x}O_{2-\delta}$, with potential sources of these changes discussed. Moreover, the microstructure of nanocrystalline $Pr_xCe_{1-x}O_{2-\delta}$ is observed to have excellent stability at working temperatures below 800 °C, enabled by the inherent microstrain in the structure, highlighting the potential application of this material for solid state electrochemical devices.

© 2011 Elsevier B.V. All rights reserved.

## 1. Introduction

Undoped and doped ceria ($CeO_2$) exhibit a range of interesting properties including high oxygen ionic conductivity, extensive deviations from stoichiometry, associated mixed ionic electronic conduction and chemical expansion at reduced oxygen partial pressure, $P(O_2)$, defect association/dissociation reactions, chemical stress and strain effects [1–4]. The high ionic conductivities of acceptor doped ceria at intermediate temperatures and reduction/oxidation behavior suggest them as promising candidates for various applications such as solid oxide fuel cell (SOFC) components [5], oxygen sensors [6] and catalysts [7], respectively. In addition, ceria is a model material for investigating fundamental questions regarding the interaction of defects, and the relationship between residual stresses and defect equilibria given its high melting point and simple fluorite structure [1,2].

In the fuel cell application, $CeO_2$-based oxides are exposed to both highly oxidizing and reducing conditions. It is therefore important to understand how $CeO_2$-based oxides behave chemically, mechanically and microstructurally under these conditions. In addition, some nanocrystalline ceramics have recently been reported to exhibit superior transport properties compared with coarse-grained materials [8,9]. This has been attributed to the high defect densities and/or fast diffusion pathways (i.e. surfaces and grain boundaries) characteristic of nanocrystalline materials [8,9]. In order to improve our understanding of the potentially promising properties of nanocrystalline ceria-based materials for SOFC applications, their chemical and mechanical properties as well as their microstructural stability under working conditions (*e.g.* temperature and $P(O_2)$) need to be systematically studied. We have, therefore, as part of a more extensive examination of the electrical, mechanical and defect properties of $Pr_xCe_{1-x}O_{2-\delta}$ over a wide range of temperature and $P(O_2)$, undertaken, in the present work, the investigation of the chemical expansion, thermal expansion and microstructural stability of nanocrystalline $Pr_xCe_{1-x}O_{2-\delta}$ powders by *in situ* X-ray diffraction (XRD) between room temperature and 1075 °C in air.

## 2. Experimental

Nanocrystalline $Pr_xCe_{1-x}O_{2-\delta}$ (PCO) powders were synthesized by a Pechini-type sol-gel process allowing for the preparation of muticomponent oxides with homogeneous distribution of the constituent metal ions at the molecular level [10,11]. Cerium (III) nitrate hexahydrate (99.99%; Sigma Aldrich), praseodymium (III) nitrate hydrate (99.9%; Alfa Aesar), ethylene glycol (99%; Alfa Aesar) and citric acid anhydrous (Fisher Scientific) were used to prepare PCO solid solutions with $x = 0.01$, 0.1 and 0.2. Aqueous solutions of cerium (III) nitrate and praseodymium (III) nitrate were mixed together by stirring. Thereafter, citric acid and ethylene glycol were added into the solution to form a gel. The mole ratio of citric acid to metal ion was 2:1. The resultant mixtures were stirred at 80 °C until polyesterification between the citric acid and ethylene glycol formed a dry gel. After

* Corresponding author at: Department of Materials Science & Engineering, Massachusetts Institute of Technology, 77 Massachusetts Avenue, Cambridge, MA 02139, USA. Tel.:+1 617 253 1749.
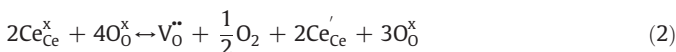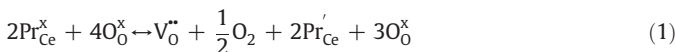*E-mail address:* ykuru@mit.edu (Y. Kuru).

being dried in an oven at 110 °C for 12 h, the powder was ground in a zirconia mortar, and then prefired at 300 and 450 °C for 4 h under air. Finally, the sample was fully calcined at 700 °C for 3 h and then milled for 12 h in isopropyl alcohol with zirconia balls.

The $2\theta$-$\omega$ scans ($2\theta$ is the angle between the incident and the diffracted X-ray beams; $\omega$ is the angle between the incident beam and the specimen surface) were carried out by a PANalytical Expert Pro MPD diffractometer equipped with programmable incident-beam divergence slits and a high-speed high-resolution X'Celerator position-sensitive detector using Cu Kα radiation. An Anton Paar HTK1200N furnace, capable of heating the specimen from 25 to 1200 °C, was mounted to the diffractometer as the sample stage during *in situ* heating experiments. The lattice parameters of the powders were determined by plotting the lattice constant, $a$, against the Nelson-Riley function and taking the intercept of the line fitted to the data [12]. A representative example demonstrating the quality of the fit can be seen in reference [13]. The crystallite size, $D$, and the microstrain (describing the local variations in lattice spacings), $\varepsilon$, were determined by the Williamson–Hall method [14]. Size and microstrain broadenings are assumed to be Lorentzian, and thus linearly additive in the Williamson–Hall analysis. Their differentiation is based on the dependence of each broadening type on $\theta$ [14]. In order to determine the instrumentally broadened profile of the diffractometer as a function of diffraction angle $2\theta$, 13 $hkl$ reflections of a LaB$_6$ (NIST SRM660) standard powder sample were measured.

The microstructures of the as-prepared and heat-treated $Pr_{0.2}Ce_{0.8}O_{2-\delta}$ powders were investigated in a JEOL 2010 FEG Analytical Electron Microscope operating at an accelerating voltage of 200 kV.

## 3. Results and discussion

The expansion of PCO lattice with increasing temperature, $T$, is due to two sources: (i) pure thermal expansion of the unit cell caused by the asymmetry of the potential energy curve, and (ii) chemical expansion of the unit cell due to oxygen loss from the lattice by reactions (1) and/or (2), written according to the Kröger–Vink notation [15].

$$2Pr_{Ce}^{x} + 4O_{O}^{x} \leftrightarrow V_{O}^{\bullet\bullet} + \frac{1}{2}O_2 + 2Pr_{Ce}^{'} + 3O_{O}^{x} \tag{1}$$

$$2Ce_{Ce}^{x} + 4O_{O}^{x} \leftrightarrow V_{O}^{\bullet\bullet} + \frac{1}{2}O_2 + 2Ce_{Ce}^{'} + 3O_{O}^{x} \tag{2}$$

The chemical expansion arises upon the reduction of $Pr^{4+}$ and/or $Ce^{4+}$ cations to their respective +3 valance states [16,17]. It is known that $Pr^{4\pm}$ reduces to $Pr^{3\pm}$ at lower temperatures compared to $Ce^{4\pm}$ reduction to $Ce^{3\pm}$ due to the lower enthalpy of reduction of $Pr^{3\pm}$. For example, at 1100 °C and under 200 mbar $P(O_2)$, while over 90% of $Pr^{4\pm}$ cations are reduced to $Pr^{3\pm}$, $Ce^{4\pm}$ cations do not yet reduce to $Ce^{3\pm}$ [18]. Therefore, within the temperature range of our experiments, 25–1075 °C, we believe that the measured chemical expansion arises nearly entirely from the reduction of the $Pr^{4+}$ cations.

Here, we report on the lattice parameter of nanocrystalline PCO as a function of temperature, and from this, we deduce its chemical expansion coefficient. The variation of the measured lattice parameter, $a$, with $T$ of nanocrystalline PCO powders having different Pr levels is seen in Fig. 1(a). In addition, the data reported in reference [19] for coarse-grained bulk ceria is also included in the same plot. It is evident that $a$ is nearly independent of dopant concentration below 500 °C. In addition, the lattice parameter, $a$, reported for the bulk, undoped material [19], is slightly smaller than the values obtained in the present study. This effect can be attributed to a relatively larger surface relaxation in nanocrystalline PCO compared to bulk ceria and, hence, formation of a core-shell structure in nanocrystalline PCO as mentioned in reference [20]. However, we also note that the dependence of $a$ on particle size does not always favor larger $a$ with smaller particles, and

can exhibit the opposite trend in some cases (*e.g.* as reported for some metals) due to the high Laplace pressure on nanoparticles [21].

Fig. 1(b) shows the total expansion coefficient, $\alpha_T$, defined as $\frac{1}{a} \cdot \frac{\partial a}{\partial T} = \alpha_T = \alpha_{Ther} + \alpha_{Chem}$, where $\alpha_{Ther}$ and $\alpha_{Chem}$ stand for the thermal and chemical expansion coefficients, respectively. Therefore, $\alpha_T$ represents both sources of expansion, as a function of temperature. The onset (>400 °C) and saturation (~1000 °C) of the chemical expansion component can be visualized more clearly in this figure. Based on the lower temperature of reduction of $Pr^{4+}$ compared to $Ce^{4+}$ in PCO, we assign the onset of chemical expansion component to the onset in the reduction of $Pr^{4+}$. Chemical expansion begins at 500 °C for PCO ($x = 0.1$), whereas for PCO ($x = 0.2$) the reduction of $Pr^{4+}$ cations begins at considerably lower temperatures (about 400 °C). This is consistent with a lower enthalpy of reduction in PCO with increasing Pr level [17,22]. The general trend for $\alpha_T$ observed for the nanocrystalline powders (shown here with one example for demonstration purposes) is consistent with recently obtained data for coarse-grained bulk PCO [22]. Another interesting point worth noting is the different behavior of the material during thermal expansion in the temperature ranges between 25 and 400 °C, and between 1000 and 1075 °C. These two ranges denote the temperature regions in which PCO expands only thermally since the reduction of $Pr^{4+}$ does not begin below 400 °C while nearly all of the $Pr^{4\pm}$ (*i.e.* above 80%) is converted to $Pr^{3+}$ above 1000 °C. Thus, Fig. 1(b) indicates that the thermal expansion of PCO is little affected by the solute (i.e. $Pr^{4+}$) content below 400 °C. On the other hand, the thermal expansion appears to be correlated with the Pr (*i.e.* $Pr^{3+}$) fraction above 1000 °C. It should be noted, however, that only two temperature points in this range could be obtained due to instrumental limitations. The results of similar experiments performed under relatively low oxygen partial pressures ($P(O_2)$ $\sim 10^{-3}$ mbar) are shown in Fig. 1(c). In these experiments, all $Pr^{4+}$ cations are expected to reduce to $Pr^{3+}$ at lower temperatures, and this enables more data points to be collected in the region where the reduction of the $Pr^{4+}$ cations is complete. It is evident that the same conclusion can be drawn; the thermal expansion in the high $T$ regime remains correlated with Pr fraction, x. However, the thermal expansion of PCO saturates above x = 0.1. In the high temperature regime, the Pr-concentration dependence of the thermal expansion coefficient suggests that the $Pr^{3+}$ cations have a greater impact on the host ceria lattice structure than $Pr^{4+}$ ions. This apparently results in a more asymmetric, potential energy versus interatomic distance curve leading to a thermal expansion coefficient which increases with temperature in a composition dependent way. Furthermore, there may also be contribution from the different ways that $Pr^{4+}$ versus $Pr^{3+}$ plus the oxygen vacancies distribute at low and high temperatures, respectively. Moreover, the chemical expansion co-efficients ($\alpha_{Chem} = \frac{1}{a} \cdot \frac{\partial a}{\partial \delta}$) of PCO at 1075 °C were estimated from the difference in lattice parameters of PCO ($x = 0.2$) and PCO ($x = 0.1$) powders since all the Pr dopants are reduced at these high temperatures and, hence, the change in $\delta$ is known. The resulting values of $\alpha_{Chem} = 0.072$–0.077 are in good agreement with the values measured for bulk PCO (i.e. 0.08–0.09) [22].

The variation of $a$ with $T$ for nanocrystalline and coarse-grained (grain size is larger than 1 μm, achieved by sintering the nanocrystalline powder at 1450 °C) bulk PCO ($x = 0.1$) is shown in Fig. 1(d). It is evident that the data collected for all materials match quite closely within experimental accuracy. This result is also in line with Fig. 1(a) and (b), indicating that the chemomechanical behavior of nanocrystalline and bulk PCO is practically identical in the temperature range between 25 and 1075 °C under air ($P(O_2)$ ~200 mbar). This is different from most of the studies regarding variation of physical and chemical properties with crystallite size [8,9,23–25].

In order to investigate the microstructural stability of PCO during its reduction, grain size $D$ and microstrain $\varepsilon$ were simultaneously
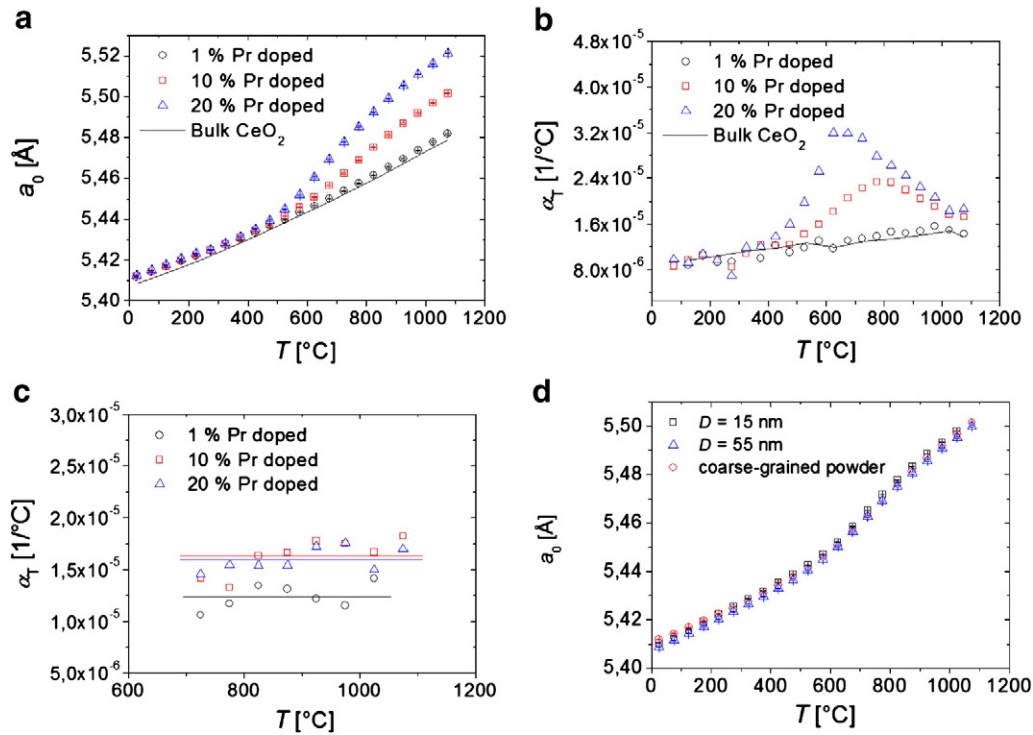
**Fig. 1.** (a) The lattice parameter, $a_0$, versus temperature, $T$, for PCO with x = 0.01, 0.1 and 0.2. The data for pure and coarse-grained ceria from Ref. [19] is also shown in the figure. (b) Total expansion coefficient, $\alpha_T$, versus $T$ for PCO with x = 0.01, 0.1 and 0.2 in air. The data for undoped, coarse-grained ceria calculated from Ref. [19] is also shown in the figure. (c) $\alpha_T$ versus $T$ for PCO with x = 0.01, 0.1 and 0.2 between 725 and 1075 °C under low $P(O_2)$ (~$10^{-3}$ mbar). (d) $a_0$ versus $T$ for nanocrystalline (i.e. $D$ = 15 and 55 nm) and coarse-grained PCO with x = 0.1. All measurements except those shown in (c) were performed in air; the error bars are on the order of the symbol size.

measured as a function of temperature. Fig. 2(a) and (b) illustrates the changes in $D$ and $\varepsilon$ of PCO (x = 0.2) powder with temperature, respectively. The specimen has ~0.15% microstrain in the as-prepared
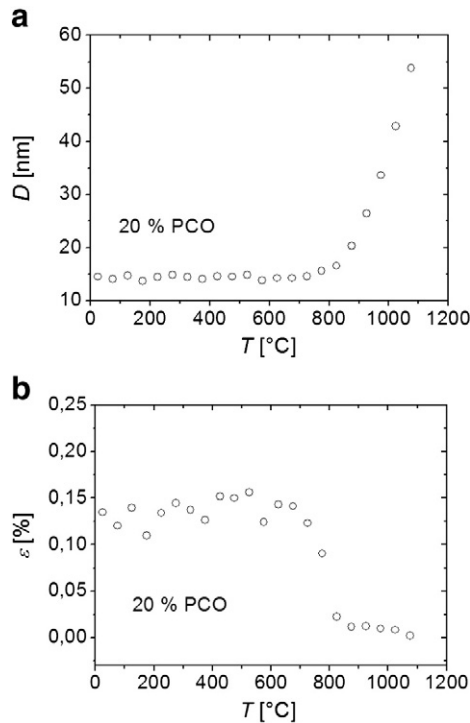


**Fig. 2.** (a) Crystallite size, $D$, versus temperature, $T$, and (b) microstrain, $\varepsilon$, versus $T$, for PCO with x = 0.2. All measurements were performed in air; the error bars are on the order of the symbol size.

state which remains approximately constant during heating up to 700 °C (cf. Fig. 2(b); each data point corresponds to 1-hour duration). Afterwards, grain growth starts at approximately 800 °C (i.e. ~0.4 $T_M$) when $\varepsilon$ is almost entirely relaxed. Both the tendency of the relaxation and its starting temperature are very similar to the data reported in Ref. [26] for Gd-doped ceria. The local distortions in the lattice, quantified in terms of the microstrain here, may be responsible for the impediment of the grain growth and its self-limited character, providing microstructural stability upon reduction. The $D$ values obtained from XRD line-broadening analysis are quite consistent with the average particle sizes obtained from transmission electron microscopy (TEM) experiments. The TEM images of the as-prepared and heat-treated PCO with x = 0.2 powders are shown in Fig. 3(a) and (b) as examples; both methods result in as-prepared and heat-treated approximate grain sizes of 15 and 55 nm, respectively.

## 4. Conclusions

In conclusion, the variation of the lattice parameter of nanocrystalline PCO powder with $T$ and its connection to the chemomechanical behavior of PCO were measured in air and at reduced $P(O_2)$ by *in situ* X-ray diffraction for the first time. In addition, the microstructural stability was simultaneously evaluated employing X-ray diffraction line-broadening analysis. After comparing these results with the ones obtained on the coarse-grained material, the chemomechanical properties were found to be rather similar to the properties of the coarse-grained counterpart. The thermal expansion of PCO showed two distinct characteristics below 400 °C and above 1000 °C, where chemical expansion was inactive. This effect was attributed to the different behavior and/or distribution of $Pr^{4+}$ and $Pr^{3+}$ cations in the ceria lattice in the two temperature regimes, and the resultant modification of the asymmetry of the potential energy versus interatomic distance curve. The microstructure of the nanocrystalline powders was observed to remain unchanged up to 800 °C in air during reduction.
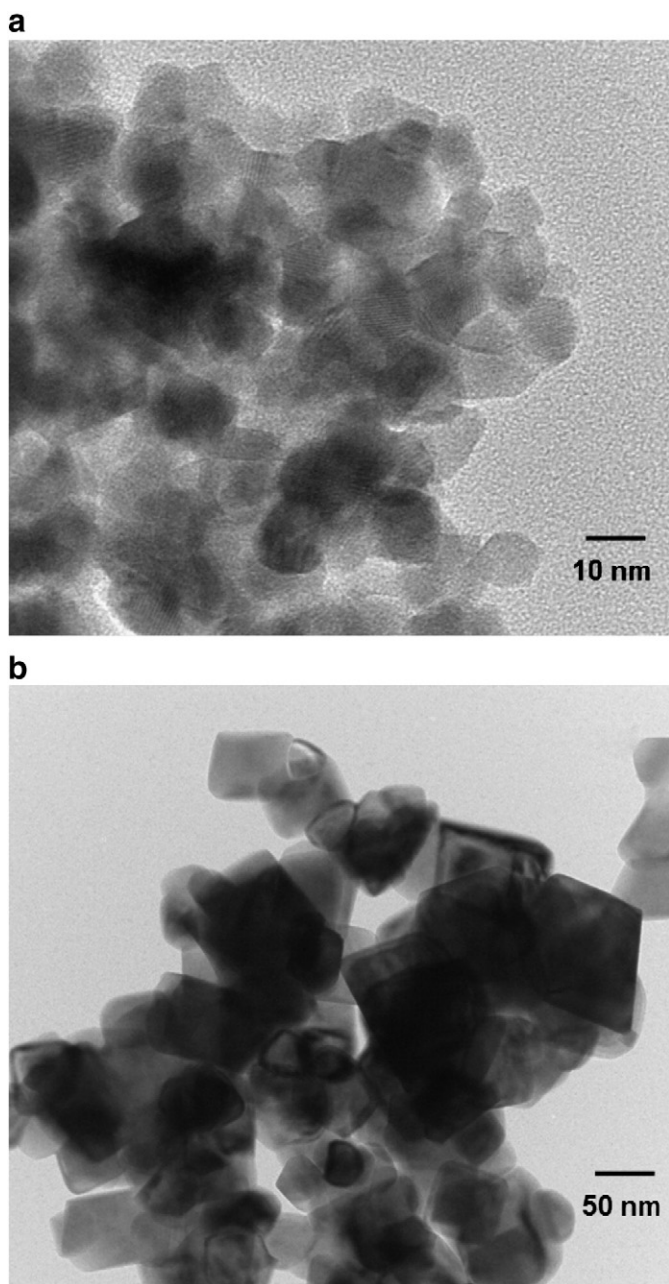
Fig. 3. TEM images of the as-prepared and heat-treated PCO with x = 0.2 powders.

The favorable amount of oxygen vacancies in PCO lattice upon reduction and its microstructural stability render PCO a promising candidate for SOFC components and open the way for more detailed investigations regarding the electrical, mechanical and defect properties of PCO in wide ranges of temperature and $P(O_2)$ which are presently underway.

Supplementary materials related to this article can be found online at doi:10.1016/j.ssi.2011.04.012.

## Acknowledgments

## References

[1] A. Kossoy, Y. Feldman, R. Korobko, E. Wachtel, I. Lubomirsky, J. Maier, Adv. Funct. Mater. 19 (2009) 634.
[2] A. Kossoy, Y. Feldman, E. Wachtel, K. Gartsman, I. Lubomirsky, J. Maier, Phys. Chem. Chem. Phys. 8 (2006) 1111.
[3] H.L. Tuller, Solid State Ionics 131 (2000) 143.
[4] A. Atkinson, Solid State Ionics 95 (1997) 249.
[5] A. Kossoy, Y. Feldman, E. Wachtel, I. Lubomirsky, J. Maier, Adv. Funct. Mater. 17 (2007) 2393.
[6] P.G. Bruce, Solid State Electrochemistry, first ed. Cambridge University Press, Cambridge, 1995.
[7] A. Trovarelli, Catal. Rev. Sci. Eng. 38 (1996) 439.
[8] M. Sillassen, P. Eklund, N. Pryds, E. Johnson, U. Helmersson, J. Bottiger, Adv. Funct. Mater. 20 (2010) 2071.
[9] Y.-M. Chiang, E.B. Lavik, I. Kosacki, H.L. Tuller, J.Y. Ying, Appl. Phys. Lett. 69 (1996) 185.
[10] M. Kakihana, M. Yoshimura, Bull. Chem. Soc. Jpn. 72 (1999) 1427.
[11] X. Liu, J. Lin, Solid State Sci. 11 (2009) 2030.
[12] B.D. Cullity, S.R. Stock, Elements of X-ray Diffraction, third ed. Prentice-Hall, Englewood Cliffs, 2001.
[13] See Supplementary data 1.
[14] G.K. Williamson, W.H. Hall, Acta Metall. 1 (1953) 22.
[15] Y.-M. Chiang, D. Birnie III, W.D. Kingery, Physical Ceramics: Principles for Ceramic Science and Engineering, first ed. John Wiley & Sons, Inc., New York, 1997.
[16] C. Chatzichristodoulou, P.V. Hendriksen, A. Hagen, J. Electrochem. Soc. 157 (2010) B299.
[17] C. Chatzichristodoulou, P.V. Hendriksen, J. Electrochem. Soc. 157 (2010) B481.
[18] S.R. Bishop, T. S. Stefanik, H. L. Tuller, Phys. Chem. Chem. Phys. In press, DOI: 10.1039/C0CP02920C.
[19] M. Yashima, D. Ishimura, Y. Yamaguchi, K. Ohoyama, K. Kawachi, Chem. Phys. Lett. 372 (2003) 784.
[20] M. Leoni, R. Di Maggio, S. Polizzi, P. Scardi, J. Am. Ceram. Soc. 87 (2004) 1133.
[21] P. Lamparter, E.J. Mittemeijer, Int. J. Mater. Res. 98 (2007) 485.
[22] S.R. Bishop, Y. Kuru, H.L. Tuller, Unpublished results.
[23] R. Birringer, H. Gleiter, Advances in Materials Science, Encyclopedia of Materials Science and Engineering, first ed. Pergamon Press, Oxford, 1988.
[24] Y. Kuru, M. Wohlschlögel, U. Welzel, E.J. Mittemeijer, Appl. Phys. Lett. 90 (2007) 243113.
[25] K. Dick, T. Dhanasekaran, Z. Zhang, D. Meisel, J. Am. Chem. Soc. 124 (2002) 2312.
[26] J.L.M. Rupp, A. Infortuna, L.J. Gauckler, Acta Mat. 54 (2006) 1721.